

Key Points:

- Models with constant fast or slow velocities fail to reproduce the primary structures observed in the Himalayas and southern Tibet
- Primary Himalayan and southern Tibetan structures are best replicated in the model where the velocity decreases from 10 cm yr^{-1} to below $\sim 3 \text{ cm yr}^{-1}$
- Orogenesis in the Himalayas can be summarized as (a) rapid thickening with crustal uplift, (b) widening along fold-and-thrust belts at the collisional margin, and (c) internal collapse and extension

Supporting Information:

Supporting Information may be found in the online version of this article.

Correspondence to:

B. S. Knight,
 ben.knight@curtin.edu.au

Citation:

Knight, B. S., Capitanio, F. A., Weinberg, R. F., & Dal Zilio, L. (2025). Slowing convergence controls on orogeny: A three-stage evolution of the Cenozoic India-Asia collision. *Tectonics*, 44, e2024TC008509. <https://doi.org/10.1029/2024TC008509>

Received 10 JUL 2024

Accepted 13 DEC 2024

Author Contributions:

Conceptualization: Ben S. Knight, Fabio A. Capitanio, Roberto F. Weinberg, Luca Dal Zilio

Data curation: Ben S. Knight

Formal analysis: Ben S. Knight, Fabio A. Capitanio

Funding acquisition: Fabio A. Capitanio

Investigation: Ben S. Knight

Methodology: Ben S. Knight, Fabio A. Capitanio

Project administration: Fabio A. Capitanio

Resources: Fabio A. Capitanio

Supervision: Fabio A. Capitanio, Roberto F. Weinberg

Validation: Ben S. Knight, Fabio A. Capitanio

Visualization: Ben S. Knight, Fabio A. Capitanio

Writing – original draft: Ben S. Knight, Fabio A. Capitanio

Slowing Convergence Controls on Orogeny: A Three-Stage Evolution of the Cenozoic India-Asia Collision

Ben S. Knight^{1,2} , Fabio A. Capitanio² , Roberto F. Weinberg² , and Luca Dal Zilio^{3,4} 

¹School of Earth and Planetary Sciences, Curtin University, Perth, WA, Australia, ²School of Earth, Atmosphere & Environment, Monash University, Clayton, VIC, Australia, ³Earth Observatory of Singapore, Nanyang Technological University, Singapore, Singapore, ⁴Asian School of the Environment, Nanyang Technological University, Singapore, Singapore

Abstract The Cenozoic India-Asia convergence represents the most well-documented case of long-lived orogeny, characterized by slowing plate convergence and complex deformation across the collisional margin, from crustal burial, exhumation and thrusting in the Himalaya, to thickening of southern Tibet. Here, we use a thermo-mechanical computational model to show the controls of decelerating convergence on the lithospheric and orogenic structures during prolonged collision. Constant convergence velocity models, bracketing the India-Asia convergence velocity, illustrate two rheological end-members, a fast-convergence orogeny dominated by lithospheric underthrusting and crustal burial and exhumation, and a slow convergence orogeny dominated by fold-and-thrusting and no lithospheric underthrusting. In contrast, models simulating the decelerating India-Asia convergence history show a unique evolutionary path. The initial structures formed at fast convergence are subsequently destabilized as convergence decreases below $\sim 5 \text{ cm yr}^{-1}$, and the structural style transitions from crustal burial and exhumation, and thickening to outwards compression along a frontal fold-and-thrust belt, progressively underthrusted by the subducting lithosphere. As the convergence decreases below $\sim 3 \text{ cm yr}^{-1}$, the reduced compression cannot sustain the plateau height and crustal thickness, inducing collapse of the orogen interiors and the diapiric ascent of buried crust. These models show a three-stage orogeny: fast thickening with crustal exhumation, widening along a frontal and fold-and-thrust belt, and internal collapse and extension. Similar to structuring of the Himalaya-southern Tibet, with the early rise of the southern Tibetan Plateau to the Himalayan crystallines formation, to the later thrust belt expansion and internal doming, reconcile with the three-stages orogeny, emphasizing the role of slowing convergence on orogenies.

Plain Language Summary The India-Asia collision during the Cenozoic is a well-studied example of prolonged mountain-building, marked by slowing convergence and complex deformation over the last 50 million years. This process shaped the Himalayas through deep burial and uplift of rocks and thickened the crust of southern Tibet. Using computer simulations, we investigated how decelerating convergence influenced these geological structures. Comparing models with constant and slowing convergence velocity, we found distinct outcomes. At fast rates, the collision is dominated by underthrusting, leading to deep crustal burial and crustal thickening. At slow rates, fold-and-thrust belts form without underthrusting. However, with slowing convergence, the process evolves in stages. Fast convergence initially thickens the crust and uplifts the region, but as rates drop below 5 cm yr^{-1} , the system transitions to outward compression along fold-and-thrust belts. Below 3 cm yr^{-1} , reduced stress causes the mountain interior to collapse and buried crust to rise. This study identifies three phases of orogeny: (a) rapid thickening and uplift, (b) widening via fold-and-thrust belts, and (c) internal collapse and extension. These findings align with the geological evolution of the Himalayas and southern Tibet, highlighting how slowing plate movement drives the evolution of mountain belts.

1. Introduction

Since collision of India and Asia ~ 50 Ma, plate convergence has been accommodated by the structural evolution of the Himalayan mountains and the Tibetan Plateau (DeCelles et al., 2002; Guillot et al., 2003; Molnar & Tapponnier, 1975) (Figures 1a and 1b). The convergence has been prolonged, initially marked by high convergence velocity at collision, followed by a decline (Figure 1c). This process led to the complex structuring of the collisional margin, with deformation distributed between the Himalayan mountains and the southern Tibetan plateau. These complexities are unique to this segment of the Alpine-Himalayan Cenozoic collision and many questions remain unresolved, crucial to the understanding of how plate convergence and orogeny correlate.

Writing – review & editing: Ben S. Knight, Fabio A. Capitanio, Roberto F. Weinberg, Luca Dal Zilio

The India-Asia convergence and Himalaya-Tibet structuring are the archetypical case for convergence-orogeny relation. In this area, this problem is best addressed as the combination of the India-Asia plate kinematics, how the convergence is partitioned, and the structuring of the orogeny, during the long-lived collision. However, each of these component carries broad uncertainties. The India-Asia plate kinematics has been subject to debate, mostly related to the reconstruction and dating of the Indian Ocean floor (Liu et al., 2023; Molnar & Stock, 2009; Replumaz et al., 2004; van Hinsbergen et al., 2011). A robust feature of the convergence history is the decreasing velocity throughout the Cenozoic (Figure 1c), where the convergence velocity decreases from ~ 18 to $\sim 10 \text{ cm yr}^{-1}$ before $\sim 45 \text{ Ma}$, to current rates of between ~ 2 and $\sim 5 \text{ cm yr}^{-1}$ (Gibbons et al., 2015; T.-Y. Lee & Lawver, 1995; van Hinsbergen et al., 2011). Despite the evidence for deceleration, establishing clear connections between convergence and the evolution of the Himalaya-Tibetan Plateau orogeny has been challenging (Clark & Royden, 2000; Molnar & Stock, 2009; Replumaz et al., 2004; Royden et al., 1997).

The debate on how the convergence is accommodated in the India-Asia collision is mostly related to the fate of the Indian crust, which is either subducted, accommodated within the Asian plate, or in the Himalayas. The discrepancies between convergence and the minimum Indian lithosphere subduction rate of $\sim 2 \text{ cm yr}^{-1}$ (Ader

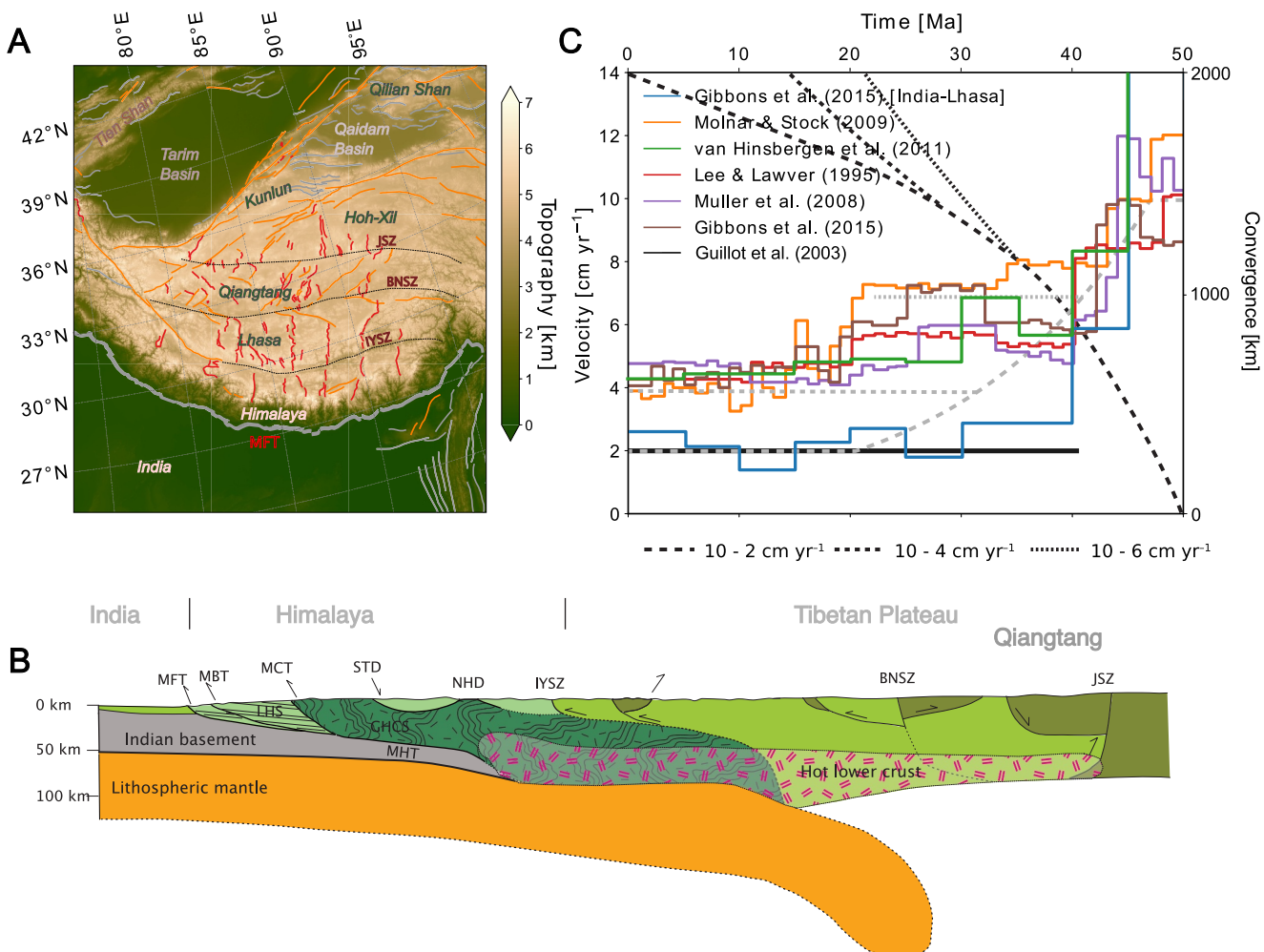


Figure 1. (a) Topography and major faulting of the Himalaya-Tibetan Plateau (Robinson et al., 2014). Normal faults in red, strike-slip faults in yellow, IYSZ Indus-Yarlung-Tsangpo Suture Zone, BNSZ Bangong-Nujiang Suture Zone, JSZ Jinsha Suture Zone, MFT Main Frontal Thrust, MHT Main Himalayan Thrust, MBT Main Boundary Thrust, STD South Tibetan Detachment, LHS Lesser Himalaya Units, GHCS Greater Himalayan Crystalline Sequence, TSS Tethyan Sedimentary Units, NHD North Himalaya Domes (Taylor & Yin, 2009). (b) Schematic cross section of the Himalaya orogen and Tibetan Plateau, modified after (Grujic et al., 2011; Searle, 2015). (c) Convergence velocities from Gibbons et al. (2015), Lee and Lawver (1995), Molnar and Stock (2009), Müller et al. (2008), and van Hinsbergen et al. (2011) and subduction velocity (black) from Guillot et al. (2003). Gray solid lines are the convergence velocity used here for the decreasing velocity models and the gray dashed lines are the corresponding total convergence.

et al., 2012), likely consistent throughout the Cenozoic (Guillot et al., 2003) (Figure 1c, black), allow for different hypotheses on continental crust accommodation. These can be solved by different time of collision and crustal thickening (Rowley, 1996), or different indentation distance (Yin & Harrison, 2000), or various extents of crust flow or thrusting toward the Asian interior (Clark & Royden, 2000; Replumaz et al., 2004; Yakovlev & Clark, 2014). However, geophysical imaging does not clearly resolve the nature of the crust in the suture zone, and whether the Indian crust is accommodated beneath the orogeny, or up to ~30% is lost to subduction (Ingalls et al., 2016; Replumaz et al., 2010; Yakovlev & Clark, 2014), remains debated, preventing quantitative reconstructions (DeCelles et al., 2001). While the exhumation of the Indian crust, or the unsubducted part of it, is a known process, how much of this is emplaced beneath southern Tibet, on the Asian upper plate, and how north, remains unknown (Jamieson & Beaumont, 2013). Additional uncertainties also affect the late-stage structuring of the Himalayas, where crustal shortening in the fold-and-thrust belt may vary largely, from ~650 to 1,000 km (DeCelles et al., 2001, 2002), even surpassing 1,300 km (van Hinsbergen et al., 2011). These figures contrast with estimates derived from plate kinematics, which suggest total convergence ranging from 2,000 to 3,600 km since 50 Ma (Molnar & Stock, 2009; van Hinsbergen et al., 2011). The discrepancies may relate to assumptions regarding the subduction history of the Indian lithosphere (e.g., Jagoutz et al., 2011) or variations in the extent and nature of the Greater Indian margin (e.g., Liu et al., 2023), and constrain the subduction rate to be ~2 cm yr⁻¹ (Ader et al., 2012), while the rest of the convergence is accommodated by indentation.

Here, we propose a test of the relation between convergence, subduction and orogeny by means of numerical modeling. We use two-dimensional computational models of convergence, subduction and collision to first show the relation among these at constant rates, then test more realistic decreasing convergence histories, further emphasized by the uniform rheology across the margin, that is, the Indian (downgoing) and Asian (upper) plates sharing the same rheology. Because the strength of rocks depends on the temperature- and strain rate (e.g., Faccenda et al., 2009; Knight et al., 2021; Piccolo et al., 2017; Vogt et al., 2017), constant convergence velocity models illustrate two end members orogens, one dominated by high internal shear, burial and exhumation at faster convergence, the other controlled by folding and thrusting at slower rates. These two end members are both represented in orogenies (Faccenda et al., 2008; Jamieson & Beaumont, 2013; Knight et al., 2021) therefore the structure of the Himalayas must be captured by modeling a more realistic decreasing convergence. Decelerating convergence results in evolving structures and a remarkably different evolution, where early formed structures are destabilized, reactivated or abandoned, as the convergence slows. In the models, after initial crustal thickening at a high convergence velocity, the relaxation of the compression, due to the slowing convergence to rates of <~5 cm yr⁻¹, results in the formation of a fold and thrust belt extending outwards. When convergence slows to <~3 cm yr⁻¹, an additional phase is shown, with a final internal extensional period due to collapse of the plateau resulting in doming, and the continued widening of the fold-and-thrust belt. A comparison with the Himalaya-southern Tibet tectonics shows the role of convergence history on the three main stages of this orogeny, and how our models address open questions on the evolution of this unique collisional margin.

2. Modeling Convergence and Collisional Orogeny

To model the evolution of orogenic belts, we employ a numerical approach that accounts for the balance of forces from subduction, buoyancy, and internal stresses due to viscous and plastic deformation. It also considers the thermal balance between radiogenic heat production, advection, and diffusion during convergence, as well as mass transfer due to erosion and sedimentation (e.g., Gerya et al., 2008; Kelly et al., 2019; Vogt et al., 2017). We utilise the Underworld2 code, which uses a Eulerian finite element method with Lagrangian particles to solve for the viscoplastic flow of rocks (Beucher et al., 2019; Mansour et al., 2020).

The convergence of two continental plates begins at the initial collision, separated by a predetermined weak zone of lower rheological strength than the surrounding mantle that favors subduction (Figure 2a). During convergence, the crust decouples from the subducting mantle lithosphere causing crustal shortening and thickening, that is, orogeny. Convergence is modeled by imposing a horizontal convergence velocity v_c across the crust and lithosphere on the left wall of the domain, as outlined in Knight et al. (2021). Constant velocity models of $v_c = 10$ and 2 cm yr⁻¹, bracketing the inferred India-Asia motions, are compared with a model where the convergence velocity varies between these values (Figure 1c, gray solid line). All models run until a minimum convergence of 2,000 km is

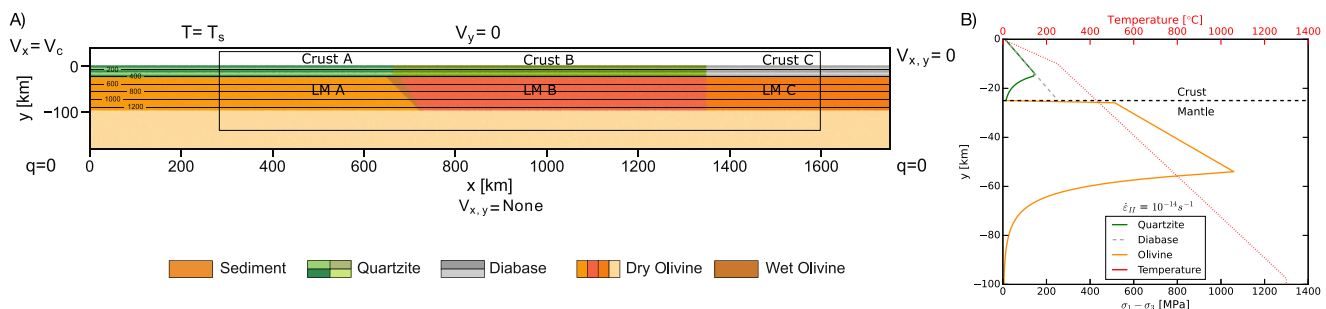


Figure 2. (a) Model setup. The convergence is applied to the left boundary of the lithosphere and crust, imposing $v_x = v_c$, with inflow and outflow across the sticky air layer. The top boundary is free slip, the right boundary no slip and the bottom boundary is unconstrained. The left, top and right boundaries have zero heat flux, whilst the temperature of the bottom boundary is unconstrained. The black box marks the area shown in subsequent figures. LM = lithospheric mantle. (b) Strength and temperature profile displaying the difference in strength between crust A/B (quartzite) and C (diabase) above 25 km depth, with a dry olivine lithospheric mantle below, at constant strain rate of $\dot{\epsilon}_H = 10^{-14} \text{ s}^{-1}$. The varying plastic strength between the crust and mantle is due to different friction coefficients (0.3—crust, 0.6—mantle).

accommodated, comparable to the India-Asia Cenozoic convergence and the reconstructed continental margin (Guillot et al., 2003; Liu et al., 2023).

The crust around the margin is not differentiated, to emphasize the role of convergence velocity. Therefore, crust A and crust B have the same rheology, where crust A represents Indian and crust B represents Asian/south Tibetan crust. Using the same rheology allows the structures to emerge based on the strain-rate dependence of the creep rheology rather than strength contrasts between the Indian (crust A) and Asian/Tibetan crust (crust B). The creep and plastic rheology of these crusts is the same, with a quartzite creep law used for crust A and B. We add a “back-stop” (crust C) by using a different crustal rheology in a distal crustal block C. Here, a diabase rheology is used for crust C (Table S1 in Supporting Information S1), making it “stronger,” that is more viscous, and is included to stop flow toward the back wall of the model. Plastic strain weakening is included, where the cohesion and friction coefficient decrease as plastic strain accumulates due to deformation. Sedimentation and erosion are included through a diffusive surface, with a constant value of $150 \text{ m}^2 \text{ yr}^{-1}$ (Text S3 in Supporting Information S1). The complete model setup and rheological laws are detailed Texts S1–S3 in Supporting Information S1.

3. Convergence History Controls on Orogeny Structures

Two end-member models are presented to explore the role of constant convergence velocity on the evolution of orogenic structures. We test a high constant convergence velocity, akin to the late Paleogene India-Asia motions, and a low constant convergence velocity, similar to the Neogene India-Asia motions, to examine the different structures that emerge when these velocities are sustained over 2,000 km of convergence. A third model category is tested with decreasing velocity, comparable to the convergence history between India and Asia, to see how structures emerge and reorganize due to the decreasing convergence velocity. Because of the uncertainties of the partitioning of the current convergence, we test the decrease from 10 cm yr^{-1} to a minimum velocity varying from 6, to 4 and 2 cm yr^{-1} , which bracket the proposed values and allow to determine the sensitivity of the orogen reorganization to the decaying convergence.

3.1. Fast Convergence Model

In the fast convergence model 2,000 km of convergence is achieved at a constant rate $v_c = 10 \text{ cm yr}^{-1}$ over 20 Myr. This model results in an orogen characterized by predominant basal shearing, crustal burial beneath the upper plate and exhumation. This model forms a flat plateau with steep sloping flanks, underthrusted by the subducting lithosphere (Movie S1 in Supporting Information S2).

In the initial stage of the collision, the crust of both plates folds to form a proto-wedge (Figure 3a), and by ~ 8 Myr, it is thrust over the incoming crust. The downgoing crust reaches depths of ~ 50 – 60 km (Figure 3b), which then decouples from the subducting lithospheric mantle and injects along the upper plate's Moho boundary (Figures 3b and 3c), uplifting the overriding crust to form a plateau. The deformation is driven by the basal shearing, which weakens the crust and forces flow as it thickens and heats up.

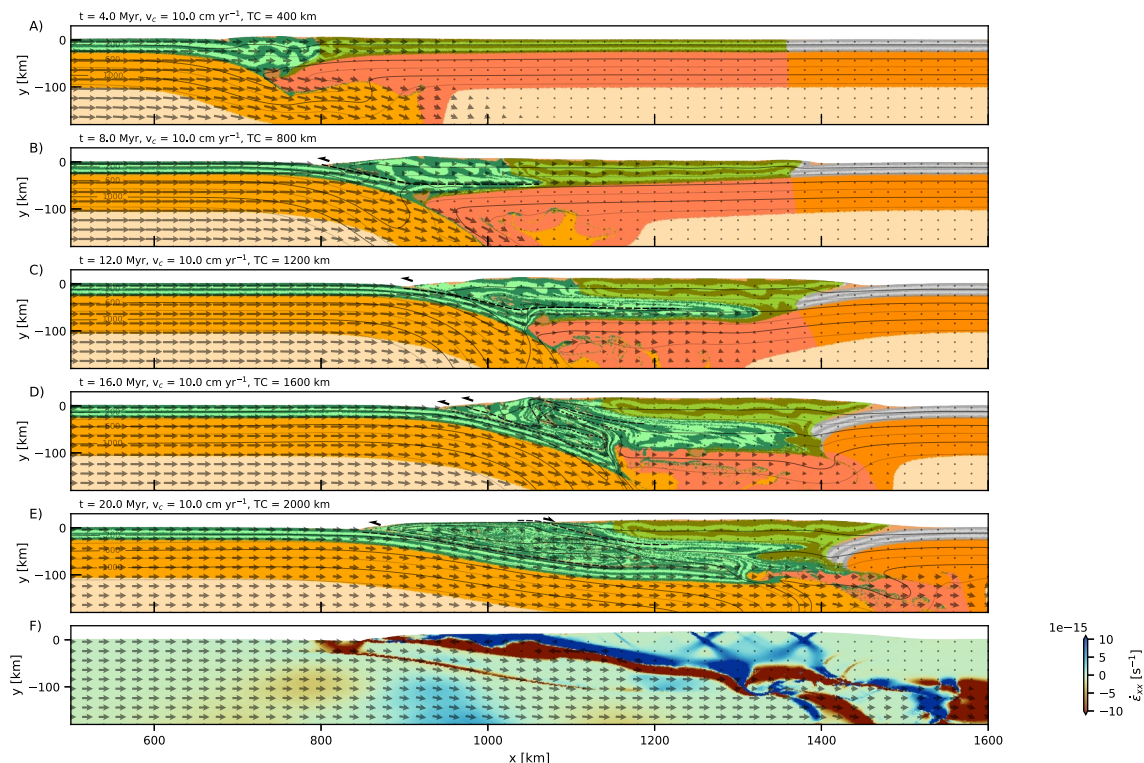


Figure 3. Fast and constant convergence velocity model $v_c = 10 \text{ cm yr}^{-1}$. Model presented at time $t = 4 \text{ Myr}$ (a), 8 Myr (b), 12 Myr (c), 16 Myr (d) and 20 Myr (e). v_c is convergence velocity (constant) and TC is total convergence. Materials as in Figure 2. (f) Horizontal strain rates $\dot{\epsilon}_{xx}$ indicating compression ($\dot{\epsilon}_{xx} < 0$) and extension ($\dot{\epsilon}_{xx} > 0$).

Once $\sim 600 \text{ km}$ of convergence is accommodated, the downgoing crust reaches $\sim 100 \text{ km}$, and is then exhumed toward the orogeny front (Figure 3, 16 Myr). The uplifted plateau acts as a rigid buttress, and cold material is subducted at the front of the orogen. As this crust subducts, it heats up, resulting in a lower density and reduced viscosity, which causes the resurfacing of incoming crust to the front of the orogen through a return (counter) flow, at velocities similar to the convergence velocity. The expanding exhumation channel gradually removes most of the proto-wedge units (Figures 3d and 3e). By the end of the model, the plateau's crust reaches a thickness of $\sim 90 \text{ km}$, where extant folded crust is stacked above the Indian crust, injected in the early (Figure 3e) and late stages. Minor translation of the orogeny over the upper plate interior occurs over a steep inward-dipping thrust.

The final topography shows a plateau approximately 7 km high and 700 km wide (Figure 3e), sloping toward the foreland, with no thrust-and-fold belt forming at the orogen front. The effects of erosion and sedimentation are minor due to the short duration of the model (20 Myr) in comparison to the other models (100 Myr—slow, 50 Myr—decelerating), with only small amounts of sediment deposited across the plateau. As the fast convergence persists, isotherms are drawn to shallow depths in the exhumation channel, bordered by a cooler plateau interior.

The late stage of this model shows the deep underthrusting of crust A to $\sim 170 \text{ km}$ past the suture zone (Figures 3e and 3f), with the majority of deformation occurring along this shear zone (Figure 3f). This is mostly accommodated by compression along the base of the return flow region, indicated by strain rates $\dot{\epsilon}_{xx}$ in excess of 10^{-15} s^{-1} (Figure 3f) and extension along the top region of the return channel, and minor extension in the plateau. The downgoing lithosphere underthrusts the upper plate, removing (delaminating) the lithospheric mantle (LMB in Figure 2), as the dipping angle decrease and the orogeny slightly widens. Convergence is persistently accommodated by the crustal return flow (Figure 3e), entrained deeply beneath the plateau reaching UHP conditions, that is $>2.5 \text{ GPa}/800^\circ\text{C}$, while the plateau interior experiences minimal deformation and no frontal fold-and-thrust forms.

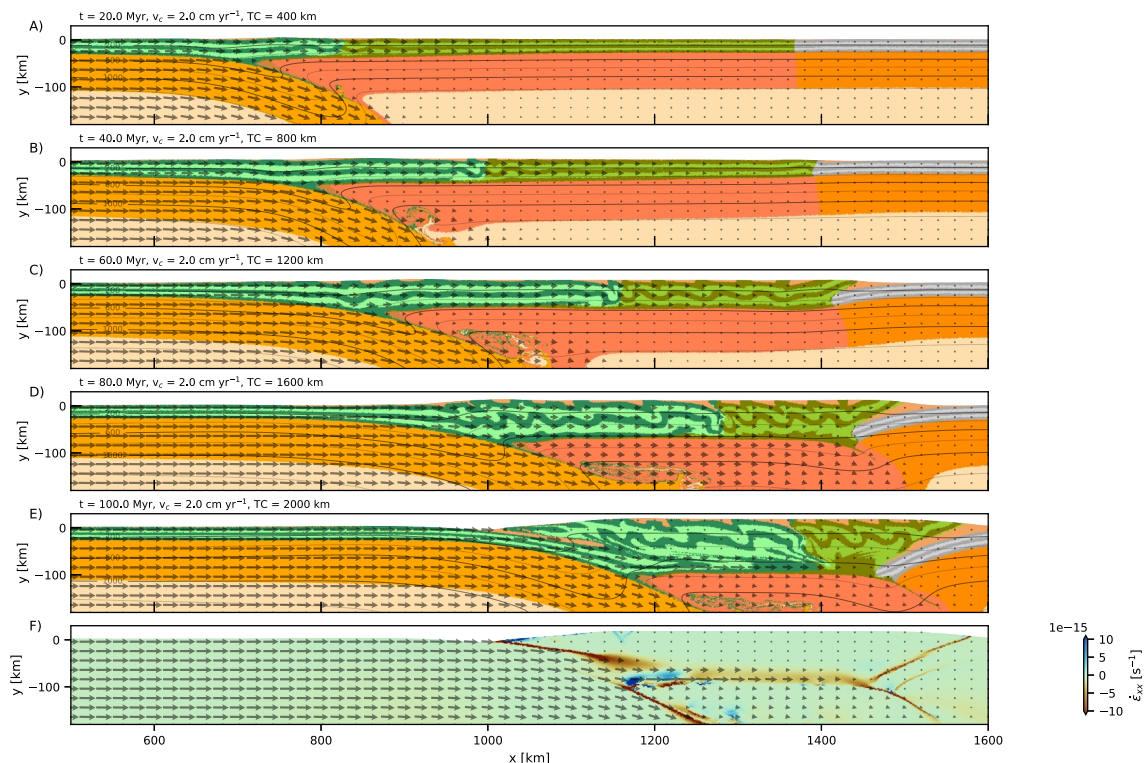


Figure 4. Slow and constant convergence velocity model, $v_c = 2 \text{ cm yr}^{-1}$. Model presented at time $t = 20 \text{ Myr}$ (a), 40 Myr (b), 60 Myr (c), 80 Myr (d) and 100 Myr (e). v_c is convergence velocity (constant) and TC is total convergence. Materials as in Figure 2. (f) Horizontal strain rates $\dot{\epsilon}_{xx}$ indicating compression ($\dot{\epsilon}_{xx} < 0$) and extension ($\dot{\epsilon}_{xx} > 0$).

3.2. Slow Convergence Model

In the slow convergence model, a constant rate of $v_c = 2 \text{ cm yr}^{-1}$ over 100 Myr achieves 2,000 km of convergence, resulting in a distinct structural style characterized by predominant pure-shear thickening, folding, and minor faulting (Movie S2 in Supporting Information S2). This forms a flat plateau with sloping flanks, similar to the fast convergence model, despite the different internal structures, constrained by the upper plate lithosphere.

Throughout most of the model duration, until approximately 80 Myr (equivalent to around 1,600 km of convergence), slow convergence is primarily accommodated by crustal folding. This sequential folding into the upper plate culminates in a cohesive crustal plateau with a uniform thickness of around 70–80 km (Figures 4c and 4d). In contrast to the fast convergence model where the short duration minimizes diffusion, thermal diffusion re-equilibrates the perturbed geotherms at the slow convergence velocity, leading to a thicker colder crust forming a fold belt, while no return flow occurs (Figure 4d). This is a consequence of the slow convergence which minimizes perturbations to the geothermal gradients within the orogeny, which becomes cooler with uniform thickening.

In the late stages (~80–100 Myr; Figures 4d and 4e), the incoming crust is deeply buried and accommodated at the base of the orogen. The thickened crust load promotes thrusting at the orogen borders and shearing of the incoming crust at the plateau's base. This is illustrated by strain rates $\dot{\epsilon}_{xx}$ and velocity vectors (Figure 4f), showing localization of compression along the outer thrusts and distributed deep crustal strain beneath the plateau, while extension within the plateau is negligible. Another important difference is that no exhumation occurs at the front of the orogen and minimal crustal flow is a late-stage and minor feature. In contrast to the fast model, the two crusts remain separated by a steep suture zone.

The orogen in this model develops a plateau, ~600 km wide and of similar elevation to the plateau in the fast model, although developing remarkably different internal structures. Erosion and sedimentation are intensified due to the model duration, though limited by the gentle slopes. Thicker sediment layers form on the plateau and

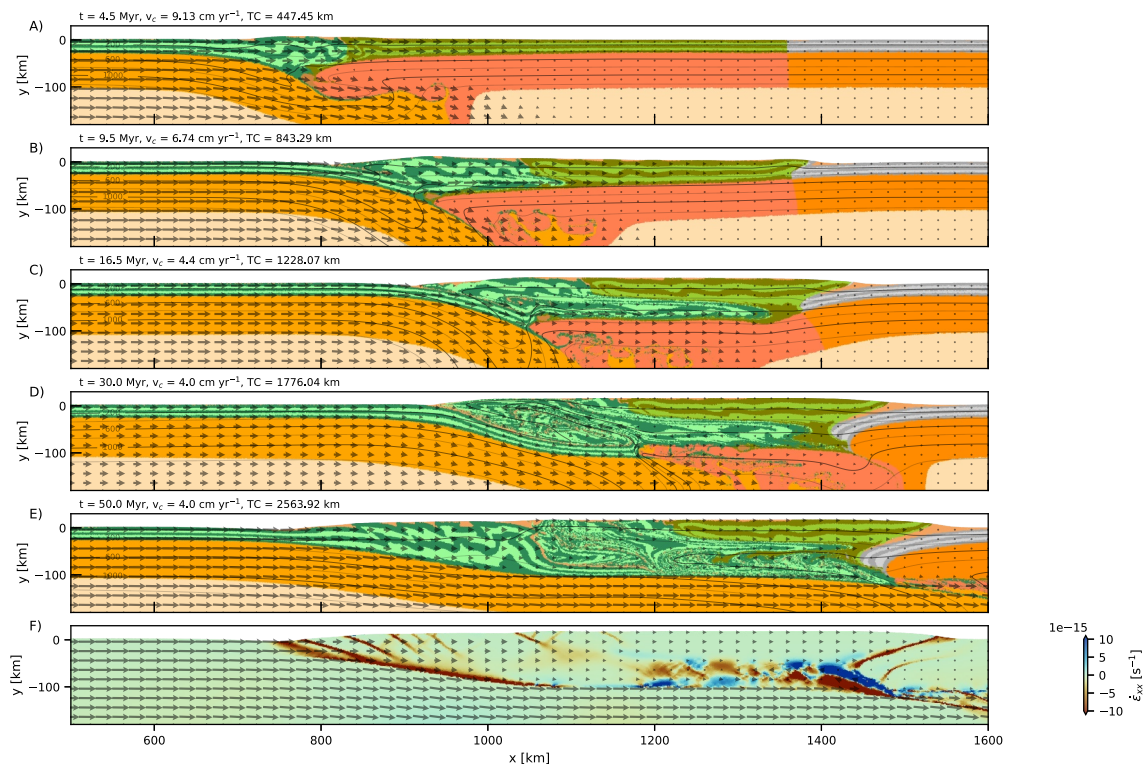


Figure 5. Evolution of decreasing convergence velocity model with velocity decreasing from $v_c = 10$ to 4 cm yr^{-1} (see Figure 1c). Model presented at time $t = 4.5 \text{ Myr}$ (a), 9.5 Myr (b), 16.5 Myr (c), 30 Myr (d) and 50 Myr (e). v_c is convergence velocity (variable) and TC is total convergence. Materials as in Figure 2. (f) Horizontal strain rates $\dot{\epsilon}_{xx}$ indicating compression ($\dot{\epsilon}_{xx} < 0$) and extension ($\dot{\epsilon}_{xx} > 0$).

are entrained in the orogen by thrusting, while crustal structures on the upper plate buttress remain similar to those in the previous model.

Lower convergence velocity coupled with reduced internal temperatures prevents the deformation of the upper plate lithosphere, which is preserved beneath the orogeny (Figure 4e) as the downgoing lithosphere subducts into the mantle beneath the orogenic front. A fundamental difference is the nature of the plateau, where the bulk of the plateau overlays a layer of crust A in the fast convergence model, while in the low convergence the two crusts are side-by-side, separated by a steep suture.

3.3. Decelerating Convergence Models

3.3.1. Convergence Decreasing to 6 cm yr^{-1}

The $10\text{--}6 \text{ cm yr}^{-1}$ decelerating model is run until 2,000 km of convergence is reached ($\sim 26.5 \text{ Myr}$; Figure 1c). This model reproduces similar structures (Figure S1 in Supporting Information S1) to the constant fast velocity (10 cm yr^{-1}) model (Figure 3), in which a proto-wedge initially forms before backward migration and thickening of the crust results in the formation of a plateau. The continued convergence results in the subduction of lower crust (crust A) that eventually returns to the surface in a return flow pattern, along an exhumation channel (Movie S3 in Supporting Information S2).

3.3.2. Convergence Decreasing to 4 cm yr^{-1}

The $10\text{--}4 \text{ cm yr}^{-1}$ decelerating model is run for 50 Myr (Figure 1c) and results in $\sim 2,570 \text{ km}$ of convergence (Movie S4 in Supporting Information S2), compatible with estimates of the length of the Greater Indian extended margin (Meng et al., 2019).

In the initial stage, deformation of the crust is comparable to that in the fast-convergence model, with folding and thrusting of an initial proto-wedge (Figure 5b), followed by injection of incoming crust into the plate, $\sim 200 \text{ km}$

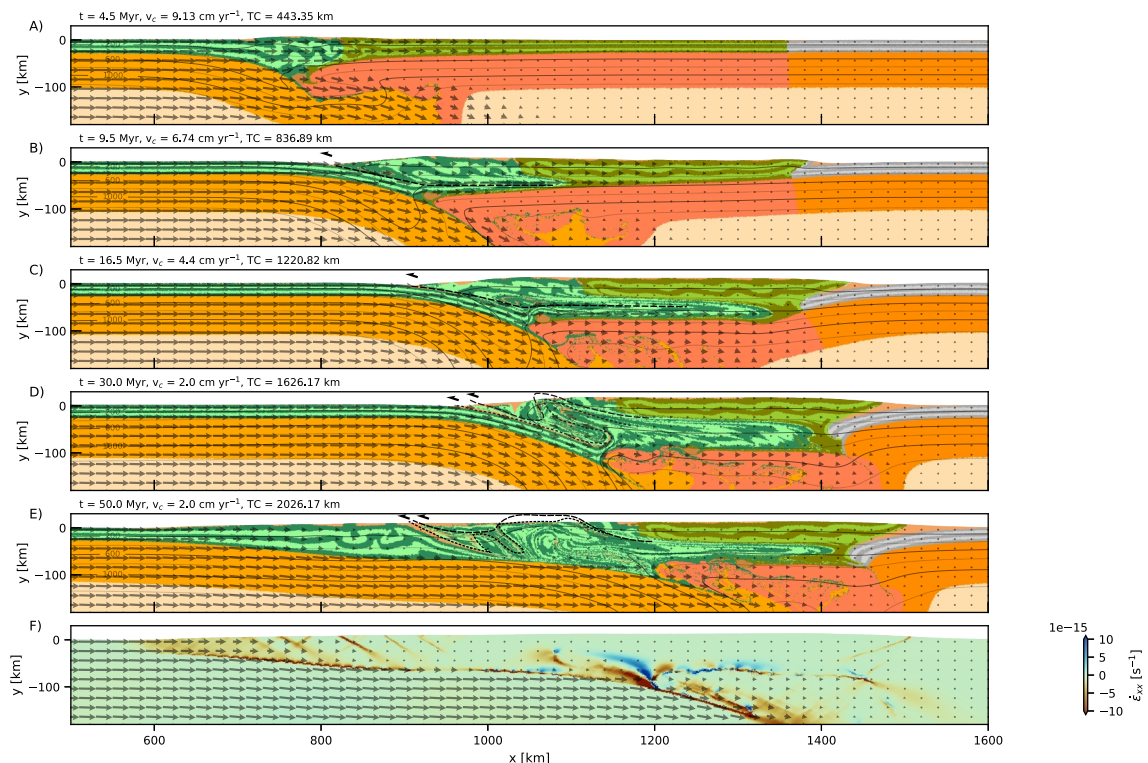


Figure 6. Evolution of decreasing convergence velocity model with velocity decreasing from $v_c = 10$ to 2 cm yr^{-1} (see Figure 1c). Model presented at time $t = 4.5 \text{ Myr}$ (a), 9.5 Myr (b), 16.5 Myr (c), 30 Myr (d) and 50 Myr (e). v_c is convergence velocity (variable) and TC is total convergence. Materials as in Figure 2. (f) Horizontal strain rates $\dot{\epsilon}_{xx}$ indicating compression ($\dot{\epsilon}_{xx} < 0$) and extension ($\dot{\epsilon}_{xx} > 0$) at final timestep.

along the Moho (Figure 5c, 16.5 Myr). Subsequently, as in the fast convergence model, the incoming crust is buried deeper, to $\sim 100 \text{ km}$ (Figure 5d, 30 Myr), then exhumed by return flow due to the heating of the crust that decreases its density and viscosity and is no longer injected beneath the plateau. The return flow to the surface forms part of the proto-wedge, with deeply buried rocks subsequently exhumed to the surface.

As the model progresses, decelerating convergence induces unique structural reorganization and outward deformation migration in the form of a fold and thrust (FAT) belt (Figure 5e). During this stage, approximately 800 km of convergence is accommodated between 30 and 50 Myr. The incoming crust, no longer buried deeply, decouples from the lithospheric mantle at $\sim 50 \text{ km}$ depth and accretes at the front of the orogen, forming a broadening frontal FAT belt. After 50 Myr the entire orogen is still under compression, which can be seen in the horizontal strain rates $\dot{\epsilon}_{xx} < 0$ (Figure 5f) across both the fold-and-thrust belt and the plateau and has a similar thickness (90 km) to the fast convergence models. In this case, most deformation is accommodated at the front of the orogen with the fold-and-thrust belt growing outwards, as opposed to the slow convergence model, where the shortening and thickening occurs in the orogen interior. By the end of the model, the width of the orogen has expanded to $\sim 750 \text{ km}$ (Figures 5e and 5f, 50 Myr).

3.3.3. Convergence Decreasing to 2 cm yr^{-1}

The $10\text{--}2 \text{ cm yr}^{-1}$ model (Movie S5 in Supporting Information S2) follows a similar evolution to the $10\text{--}4 \text{ cm yr}^{-1}$ model (Movie S4 in Supporting Information S2), with a proto-wedge forming (0–5 Myr) that migrates backwards (5–10 Myr) and results in the formation of a plateau (Figures 6a and 6b), then subsequent subduction of lower crust and injection below the plateau (10–20 Myr; Figure 6c). Once injection ceases, return flow occurs at the front of the orogen (20–35 Myr; Figure 6d), before migrating toward the foreland and the formation of a fold and thrust belt (30–50 Myr; Figure 6e). However, there is one major difference in the evolution in which the plateau is not under compression throughout and instead is under extension after $\sim 30 \text{ Myr}$, resulting in the collapse of the plateau and decrease in plateau thickness (Figure 6e).

Relaxation of stresses due to the lower convergence rate results in the collapse of the plateau and outward growth of the orogen. Channel flow ceases by ~35 Myr due to the decreasing convergence velocity stopping the burial of crustal material at the front of the orogen. The reduced velocity results in a shallowing of the brittle-ductile transition, reducing the strength of the crust which decreases the thickness of crust that can be supported, resulting in the gravitational collapse of the orogen, causing extension. This is coupled with diapiric ascent of newly weakened deep crust into the exhumed crust above (Figure 6e), promoted by the gravitational collapse of the orogen as well as the warming of the crust in that region that decreases the density of the material, which is not observed in the 10–4 cm yr⁻¹ model. This process is passive, as the flow in the exhumation channel has ceased, indicated by the vanishing of velocity vectors in Figure 6e ($x = 1,000\text{--}1,200$ km) and strain rates in the previously active basal flow region. Higher deformation rates in the ascending diapir and neighboring return flow illustrate the activity of these structures, as well as the active faulting and folding at the front and back of the orogen, as in the slow constant convergence model.

The final topography in this model has similar features to the previous models, with a flat plateau and a sloping orogenic front and rear structures (Figure 6e), however, the plateau thickness has decreased by ~20 km and the entire orogen is wider by ~100 km compared to the 10–4 cm yr⁻¹ model. The decelerating convergence rate accentuates erosion and sedimentation, allowing thicker sediment layers in the outer domains of the orogen. In this model, the plateau's lithospheric mantle is partially removed, that is, between the almost complete delamination and minor thickening of the fast and slow convergence models, respectively.

To summarize, the decelerating models illustrate that the reorganization of the orogen begin as convergence velocity declines below ~5 cm yr⁻¹. The model with a final velocity of 6 cm yr⁻¹ exhibits a structural pattern like that of the high constant (10 cm yr⁻¹) velocity model, therefore shows no transition. Instead, the 4 cm yr⁻¹ model (Figure 5e) has a similar overall structural style of the decelerating model to 2 cm yr⁻¹ (Figure 6e), showing that the transition occurs at ~5 cm yr⁻¹. Importantly, the model decelerating to 4 cm yr⁻¹ achieves no orogeny relaxation, no diapiric ascent and doming and a thicker crust portion of the crust remains buried beneath the plateau. This implies that final convergence velocity of 4 cm yr⁻¹ reduces compression due to incoming crust, leading to the transition from exhumation-dominated to fault-and-thrusting, although the compression remained sustained and is, instead, relaxed at lower velocity. The collapse of the plateau requires slower convergence (<3 cm yr⁻¹) that reduces the strength of the crust by decreasing the depth of the brittle-ductile transition, where the crust is able to support the thickness of crust formed at higher convergence rates. These results illustrate the three-stages of orogeny, which may occur as convergence slows: thickening and exhumation, frontal widening by frontal fold-and-thrust accretion, and final thinning and internal extension due to gravitational collapse.

4. Discussion

4.1. Reconciling the Himalaya-Southern Tibet Three-Stage Structuring With Convergence

Comparing models with the collisional margin of the Himalaya-southern Tibet offers insights into the joint evolution of the region, its relationship with the forming plateau and plate motions, substantiating the discussion of present-day deformation in the region. It is important to note that we do not address the whole Himalaya-Tibetan Plateau region, but we focus on the structuring and structural relation of the two, therefore only address the Himalaya-southern Tibet area, that is the area around the suture zone between the plateau and the orogen. For practical reasons, we refer to this as the Tibetan Plateau (TP).

In assessing the role of convergence velocity, only the model with a decelerating convergence velocity below ~5 cm yr⁻¹ replicates the first-order features of the India-Asia collisional margin, with the velocity decreasing to 2 cm yr⁻¹ best matching the timing of emerging features in the orogen. We therefore use the remainder of this section to support the evidence for a three-stage orogenic structuring of the region.

The Himalayan units belonging to India and the Asian units forming the Tibetan Plateau (Figure 1) are divided by the Indus-Yarlung-Tsangpo suture (IYSZ), separating thickened crust to the north, from the Himalayan fold-and-thrust belt (H-FAT), which has comparable structures all along the chain front (DeCelles et al., 2002). The development of the H-FAT belt is well constrained, with active faulting younging to the south (DeCelles et al., 2001; Goscombe et al., 2018), now active along the Main Boundary Thrusts (MBT). The H-FAT extends ~400 km from the front to the IYSZ above the Indian plate, underlain by a single, continuous seismic reflector (Gao et al., 2016), which dips gently beneath the orogen and deepens further north along a step, reaching the IYSZ

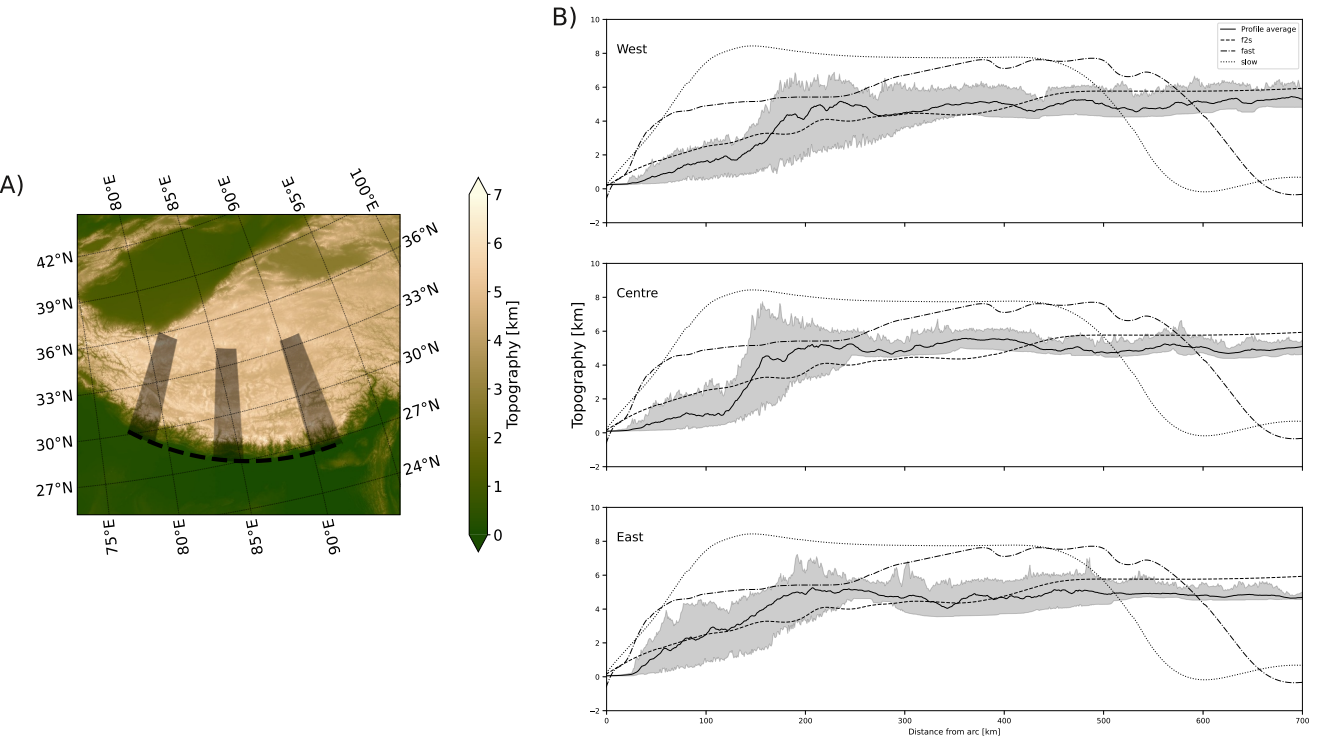


Figure 7. (a) Topographic map of the Himalayan-Tibetan region (Robinson et al., 2014). (b) Minimum, maximum and average topographic (Robinson et al., 2014) profiles from the West, center and Eastern regions (gray boxes in a) compared against model results.

(DeCelles et al., 2001, 2002; Nelson et al., 1996; W. Zhao et al., 1993). The H-FAT is overthrust along the Main Central Thrust (MCT) by the Greater Himalayan Crystalline Sequence (GHCS), where deep-seated crustal rocks have been exhumed in a channel (Beaumont et al., 2001; Grujic et al., 1996). These are overlain by the Tethyan Sedimentary Sequence (TSS), along the South Tibetan Detachment (STD) (DeCelles et al., 2001), which remained structurally high in the edifice since collision inception.

The decelerating models that decrease below 5 cm yr^{-1} reproduce these structures, including the frontal FAT belt beneath a wedge of complexly deformed and exhumed deep crustal rocks, similar to the GHCS, and topped by proto-wedge units, akin to the TSS. Except for the TSS, the other features are not captured by constant convergence models, which either do not develop a FAT belt, when too fast, or do not develop exhumation of deep rocks when too slow. The final width of the FAT in the model is $\sim 400 \text{ km}$, in agreement with the width of the H-FAT, and reproduces the deep structure of the Indian lithosphere and orogen, with folding-and-thrusting above a step-like basal decollement reaching $\sim 70 \text{ km}$ depth beneath the suture zone, then plunging into the mantle (W. Zhao et al., 1993).

The TP extends far into the Asian plate, having widened with the evolution of the orogeny (Tappannier et al., 2001). Immediately north of the IYSZ is the Lhasa Terrane (Figure 1a), $\sim 500\text{--}700 \text{ km}$ wide, supported by a $\sim 60\text{--}80 \text{ km}$ thick crust (Kumar et al., 2019). The Lhasa Terrane is underplated by Indian crust (DeCelles et al., 2002; Kumar et al., 2019; Streule et al., 2010), $\sim 200\text{--}400 \text{ km}$ further north than the IYSZ (Figure 1b). The models reproduce this geometry with accommodation of incoming crust below the Moho of the extant crust, $\sim 200 \text{ km}$ from the suture zone at the surface, uplifting a plateau with a similar crustal thickness and elevation to the TP, during the fast-converging stages, however a plateau thicknesses of $\sim 70 \text{ km}$ is only achieved after gravitational collapse of the plateau in the $10\text{--}2 \text{ cm yr}^{-1}$. In our models, the incoming crust is emplaced along the Moho between the Asian crust and lithospheric mantle. Although underplating has been proposed for the deep structures of the TP (DeCelles et al., 2002; Kumar et al., 2019), it remains poorly constrained. We further discuss below the deeper structure of the orogen against the proposed fate of the lithospheric root of the southern TP.

The results show that the $10\text{--}2 \text{ cm yr}^{-1}$ models' topography compared to the present-day orogen shows a very similar overall pattern. A plot of three sections of the southern portion of the India-Asia collisional margin

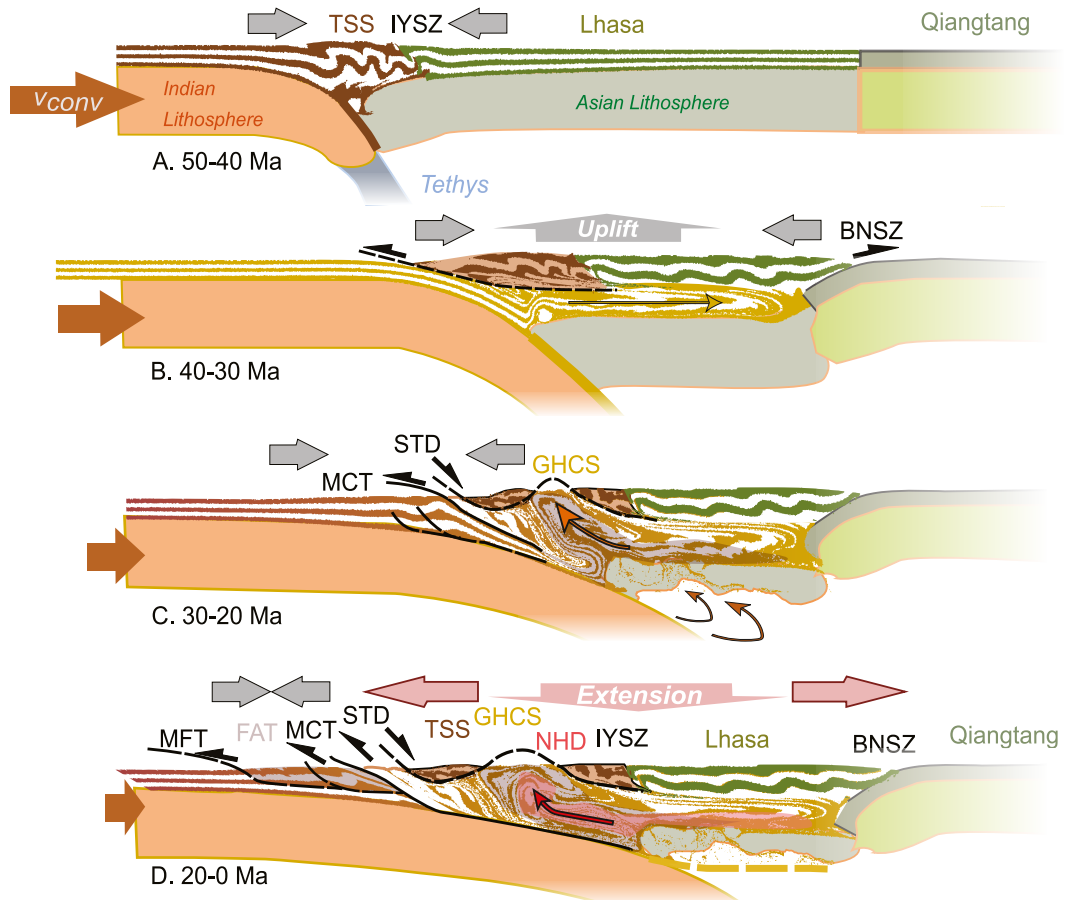


Figure 8. Sketch of the evolution of the Himalaya-Tibetan Plateau. Partially modified from Streule et al. (2010). Black lines, major tectonic contacts, colored, major units, see Figure 1.

(Figure 7a) shows an overall flat topography (Figure 7b), with consistent average elevation of $\sim 5,000 \text{ m} \pm 1,000 \text{ m}$, sloping toward the Himalayan front. The plateau can be fit similarly by the different models proposed, all reproducing a flat top and sloping flanks, however the $10\text{--}2 \text{ cm yr}^{-1}$ model topography shows an a very similar gradient at the front and reaches the average topographic height at a similar distance to the front in all three profile locations examined.

Additional support for the role of decelerating convergence to 2 cm yr^{-1} is provided by a comparison between models and evolution of the India-Asia collisional margin (Figure 8). The orogeny began with the folding of the Tethyan Sedimentary Sequence around 50 Ma (Figures 8a, TSS), which remained on top of the Himalayan sequence (Streule et al., 2010). The change of lower crust to eclogite (not included in the modeling) (Pichon et al., 1992; Spain & Hirn, 1997) supported by (ultra-)high-pressure eclogite facies found in the Kaghan area, north Pakistan, and the Tso Morari complex, NW India, suggest the Indian crust reached depths of $>50 \text{ km}$ between 47 and 43 Ma (de Sigoyer et al., 2000) (Figure 8a) before being exhumed.

The folding of the upper crust in the models matches the initial folding in the Tethyan Sequence as well as the burial of cold incoming crust to depths $>50 \text{ km}$ by $\sim 43 \text{ Ma}$ (Figures 6b and 6c), and exhumation after 34 Ma. Between ~ 40 and $\sim 30 \text{ Ma}$ (10–20 Myr after initial collision), part of the Indian crust emplaced beneath the Lhasa terrane crust (DeCelles et al., 2002; Streule et al., 2010) (Figure 8b). This process contributed to the thickening of the crust and the uplift of the TP with minimal deformation (Figure 8b). Both the fast and decreasing convergence models show similar crustal flow early in the model evolution ($\sim 7\text{--}15 \text{ Myr}$ after collision, Figures 3 and 4).

The exhumation of deep-seated Indian crust in the Greater Himalayan Crystalline Sequence (GHCS) through ductile flow (Grujic et al., 1996) (Figure 8c) is constrained by monazite U–Pb ages from ~38 Ma, although varies along the Himalaya (Finch et al., 2014; Godin et al., 2006; Goscombe et al., 2018; Searle, 2015; Searle & Hacker, 2019), lasting until the emplacement of the North Himalayan Domes, between 21 and 12 Ma (Goscombe et al., 2018), possibly subsiding when the Himalayan FAT began to develop ~18 Ma (Gao et al., 2016; Searle, 2015) until the formation of the Lesser Himalaya units (Figure 8d, LH). Both the fast and decreasing convergence models, exhibit burial and exhumation of the incoming crust. The $10\text{--}2 \text{ cm yr}^{-1}$ model shows exhumation onset by 16 Myr after initial collision and active until 42 Myr (~34 Ma, active until ~8 Ma), with the earliest shallow emplacement of exhumed units at ~25 Ma (Figures 6c and 6d). These features are consistent with long-lived metamorphism characterized by cold PT gradients, culminating in high-grade peak metamorphic conditions between ~27 and 19 Ma (Goscombe et al., 2018) and along-orogen averaged metamorphic temperatures of 600–650°C. Peak temperatures of 850°C locally found in the GHCS (Goscombe et al., 2018), are reached only for the fast convergence models, which suggests this may be due to an underestimate of the higher convergence velocities (prior to ~25 Myr) in our slowing convergence model.

After ~25 Myr, exhumation of deeply buried GHCS units and the forward migration of strain in the Himalayan front record the transition between fast and slow convergence styles. Isothermal decompression followed by rapid cooling is registered throughout much of the GHCS. The timing of the rapid cooling phase varies but is typically <20 Ma, or ~30 Myr after estimated collision (Searle, 2015). Models with decreasing convergence are the only ones that reproduce shallow rock emplacement and cooling paths, supporting the idea that exhumation is favored by slowing convergence (Maiti & Mandal, 2021). The extrusion of deep crust resulted in the emplacement of the GHCS between the STD and the MCT (Godin et al., 2006), leading to inverted metamorphic isograds above the MCT, in a “hot-on-cold” sequence (Goscombe et al., 2018; Hunter et al., 2018; Searle, 2015) and right-way-up metamorphic isograds below the STD (Godin et al., 2006; Searle, 2015) (Figure 8c). This is reproduced in all the models at high convergence velocity (Figures 3 and 6, dashed black line). The transition reflects the conditions proposed for the GHCS, with high convergence velocity required to bury rigid crust at the front of the orogen, followed by exhumation driven by released pressure gradients (Godin et al., 2006; Searle, 2015), here explained by lowered convergence velocities. Our models suggest a complex evolution of these units, in agreement with inferred post-channel, post-exhumation modifications and the TSS as a protolith for part of the GHCS (see Godin et al., 2006).

In the transitional stage of the slowing convergence models below $\sim 3 \text{ cm yr}^{-1}$, the slowing convergence allows the thermal re-equilibration of the deeply buried cold crust beneath the plateau. The ensuing warming and weakening of the deep crust and formation of buoyant, low viscosity crustal diapirs, between ~32 and ~42 Myr after collision (18–8 Ma) (Figure 8c). This mechanism aligns with the late-stage deformation of the original channel beneath the Tibetan Plateau (Jessup et al., 2006), with the Miocene doming forming the North Himalayan Domes (NHD, Jessup et al., 2019). The NHD indicates are interpreted as evidence of extension concurrent with contraction ongoing elsewhere (J. Lee et al., 2000) (Figure 8d, gray arrow for contraction, pink arrows for extension). At depth, a low viscosity, partially molten, extending from the GHCS to the Lhasa Terrane (Nelson et al., 1996; Unsworth et al., 2005), is inferred from low seismic velocity (Figure 8d). Although melting is not included in our model, the lower crust has a lower viscosity due to higher temperatures resulting in deformation in the viscous regime. It is important to note that this stage is associated with the decrease of convergence below $\sim 4 \text{ cm yr}^{-1}$, as only occurring in the models slowing to 2 cm yr^{-1} .

The ductile flow of this layer (Nelson et al., 1996) may explain the general thinning of the Lhasa Terrane's lithosphere and potassic volcanism between 30 and ~10 Ma (C. Wang et al., 2014). Thermal relaxation is a key feature of decreasing convergence models, transitioning from fast burial of cold crust to slow burial and heating due to thermal equilibration. In contrast, models with a constant convergence velocity achieve a stationary equilibrium, which may be relaxed post-orogeny. It is important to note that we do not model fluids, nor melting, but only the temperature controls on the creep, therefore we do not imply, nor require, any deep fluid or melt.

As convergence slows the orogeny reaches a new equilibrium. The India-Asia orogeny has widened through the onset of the Himalaya frontal fold-and-thrust belt above a shallow dipping lithosphere, by 32 Myr (~18 Ma, Figure 8d), then becoming the primary process accommodating convergence at 38 Myr (12 Ma) (DeCelles et al., 2001, 2002). The coeval extension along the STD as the front contracted is a known feature of the late-stage Himalayan orogeny (Burchfiel et al., 1992), captured by our models. In the Himalayan front, convergence is

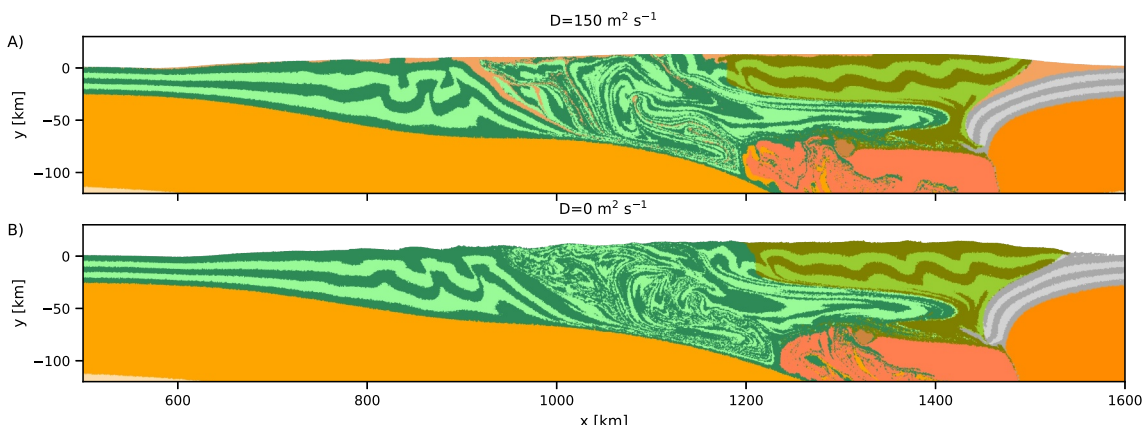


Figure 9. Comparison of the decelerating model (a) with ($D = 150 \text{ m}^2 \text{ yr}^{-1}$ —DV10-2) and (b) without ($D = 0 \text{ m}^2 \text{ yr}^{-1}$ —DV10-2_D0) sedimentation and erosion after 2,000 km of convergence over 50 Myr. All major structural features are present in both models, with some small variations due to the redistribution of material through sedimentation and erosion in (a).

currently accommodated along the Main Frontal Thrust (MFT), at rates of 2 cm yr^{-1} (Ader et al., 2012). The remainder of the convergence is likely accommodated through lateral extrusion toward east Asia and indentation (Liang et al., 2013). The FAT emerges only at slower convergence velocities ($<5 \text{ cm yr}^{-1}$) and is a result of the termination of the deep burial of crust and the cessation of return flow below. A FAT develops in both the model which decreases to 4 and 2 cm yr^{-1} at a similar time. However, the decelerating to 4 cm yr^{-1} model does not exhibit doming or relaxation due to sustained compression across the plateau and fold-and-thrust belt and features a greater crustal thickness beneath the plateau compared to that observed beneath Tibet.

4.2. Comparison With Previous Models

Although limited by the choice of two-dimensional modeling space and by the focus on the collisional margin structuring, our models illustrate realistic mechanisms that are compatible with the observables and with previous published modeling efforts. The models show that the flow of the Indian crust along the Asian Moho is a viable mechanism that occurs at high convergence velocity and is a mechanism for subsequent exhumation. In our models ~ 550 km of incoming crust can be accommodated beneath the upper plate's crust, in the early stages, between ~ 8 and ~ 20 Myr from the start of the slowing convergence models. This mechanism operates as postulated by W.-L. Zhao and Morgan (1987) and Beaumont et al. (2001) and is here reconciled with subduction dynamics. The switch from deep entrainment to exhumation in our models is due to the balance between injection pressure, due to the basal shear, and the load of the thickening plateau, then acting as a buttress, forcing the return flow to the front (e.g., Warren et al., 2008). Other studies suggest that exhumation may be driven by changes in relative plate motions, favoring relative trench motions away from the upper plate (Piccolo et al., 2017; Sizova et al., 2012). However, this constraint is relaxed if the decreasing convergence is considered, showing orogeny late-stage extension although the trench is constantly advancing in our model. Other models invoke the onset of localized erosion along the Himalayan front, to drive the frontal crust exhumation (Beaumont et al., 2001). We have tested this hypothesis with an additional model in which erosion is not accounted for (Figure 9), however the difference between this and models with erosion is negligible, supporting the idea that the pressure balance change, as convergence slows down, is a robust feature of the models.

In our models, the choice of the same crustal rheology across the margin emphasizes the role of convergence velocity, controlling the crustal effective viscosity and the rheological transition. Previous works, assuming constant convergence rate, have advocated for viscosity contrasts to explain deep burial (e.g., Piccolo et al., 2017) and flow (e.g., Royden et al., 1997). Our approach is similar; but the strength contrasts in the decelerating model presented arises as the model evolves due to decreasing convergence velocity due to the strain-rate dependent rheology and the self-organized distribution of stress within the model. The differing convergence velocities result in a range of end-member structural styles, with decreasing velocity transitioning between the two; therefore, invoking pre-collisional viscosity contrasts may be unwarranted. Our range of decelerating models show this critical transition occurs at around 5 cm yr^{-1} for the quartzite rheology utilized for the Indian and Asian

crust. Other works showed that the viscosity contrast between downgoing and upper plate's crust may limit the expansion of the orogen toward the upper plate (Chen et al., 2017; Li et al., 2016). This may indeed critically depend on the varying properties of the broad Asian lithosphere (Kelly et al., 2019), not addressed here.

The models offer insights into the fate of Asian lithosphere, which has previously been suggested to be either (partially) in place (Jiménez-Munt et al., 2008; Klemperer, 2006) or removed through delamination or subduction (Lu et al., 2018; Willett & Beaumont, 1994). The delamination of part of the Asian lithosphere has been invoked to explain the Miocene volcanism and southern Plateau uplift (Lu et al., 2018). Published models propose the advance of the subducting Indian lithosphere driving thickening of the weaker Asian lithosphere beyond stability (Kelly et al., 2019; Li et al., 2016), and the replacement in the early stages by Indian rocks beneath Tibet (Liu et al., 2023). Our models show a range of similar mechanisms, from the complete underthrusting of Asia by Indian lithosphere forcing Lhasa Terrane's lithosphere delamination, during fast convergence, to no delamination in the slow models. However, in our models this occurs as a late-stage feature, in agreement with Kelly et al. (2019), and Li et al. (2016). In summary, our models replicate these boundary conditions and suggest that convergence velocity deceleration fundamentally controls the evolution of the orogeny, potentially overstating the role of rheology differences between the Indian and Asian crust.

4.3. Speculations on the Three-Stages Himalaya-Southern Tibetan Plateau Structuring

The three stages of evolution, from the initial rapid build-up of a plateau at fast convergence to the stage of outward accretion and final internal extension stage, provide a context for interpreting the Himalayan-Tibetan Plateau's topographic evolution and its current deformation state.

Paleoaltimetry, paleobotanical, magnetostratigraphy, sedimentology, paleocurrent measurements, $^{40}\text{Ar}/^{39}\text{Ar}$ dating and fission-track studies show that the elevation of the Lhasa, Eastern Tibet and northern Qiangtang Terranes increased from $\sim 1,000$ m to $\sim 4,000$ m between ~ 50 and ~ 35 Ma (Ding et al., 2022; C. Wang et al., 2014). Our slowing convergence model supports these estimates, showing that $\sim 80\%$ of the final model topography could have been achieved early in the evolution of margin, ~ 8 – 13 Myr after collision (~ 42 and 37 Ma) due to crustal thickening (Figure 10a). A similar outcome is shown in the fast convergence model (Figure 3d), supporting the idea that early thickening of the southern Asian lithosphere may be a consequence of fast convergence.

GPS, seismic and Quaternary strain show current Plateau extension (e.g., England & Molnar, 2005), behind the compressive Himalayan front, with localized topographic lowering in the Lhasa Terrane (Q. Zhao et al., 2023). The lowering of topography is mostly explained by the extension due to the east-ward Plateau expansion (Clark & Royden, 2000), evidenced by widespread N-S trending rifts active from 19 Ma onwards (Mitsuishi et al., 2012; C. Wang et al., 2014). However, the STD and the granite-gneiss domes in the Tethyan Himalayas indicate a N-S extension event that is older than, possibly contemporaneous, with the E-W extension that formed the rifts (Mitsuishi et al., 2012). Additionally, the component analysis of current strain rate (L. Wang & Barbot, 2023) shows convergence-parallel extension localized in the Lhasa Terrane of comparable magnitude to the perpendicular extension, with this part of the extension potentially associated with the slowing convergence velocity and gravitational spreading of the plateau, as observed in the model.

Our slowing convergence model (10 – 2 cm yr^{-1}) reproduces the increase in elevation until the plateau "collapse," in the third stage, as the FAT widens (Figure 10a) which is not observed in any of the other models. The elevation reaches ~ 6.5 km, as in the constant velocity models, keeping a rather constant width (Figure 10a), equivalent to 50% of today's plateau width as measured at heights of 3 and 1.5 km. However, as deformation migrates forward to form the frontal FAT after ~ 18 Ma (Figure 10a), the plateau widens and lowers, matching the width and altitude of the Tibetan plateau today (Figure 10a). This is in agreement with paleobotanical and geological constraints on eastern Himalayan elevations, which rapidly reached $>3,000$ m starting 20–18 Ma (Ding et al., 2022) and attained comparable values to present-day by ~ 12 Ma (C. Wang et al., 2014). The altitude drops in the model by $\sim 1,500$ m between ~ 18 and ~ 8 Ma, is comparable to the inferred topographic lowering of $\sim 1,000$ m (C. Wang et al., 2014) in the plateau. The model indicates that this is due to gravitational collapse of the orogen, forming a dome region on the foreland side of the suture as compression in the interior of the orogen diminishes. This is marked by an increase in the heat flow in the orogen front (Figure 10b) and a minor increase in the inner plateau (dark green), as the FAT widens and the convergence velocity decreases below ~ 3 cm yr^{-1} . These features are not present in models with final convergence at higher rates.

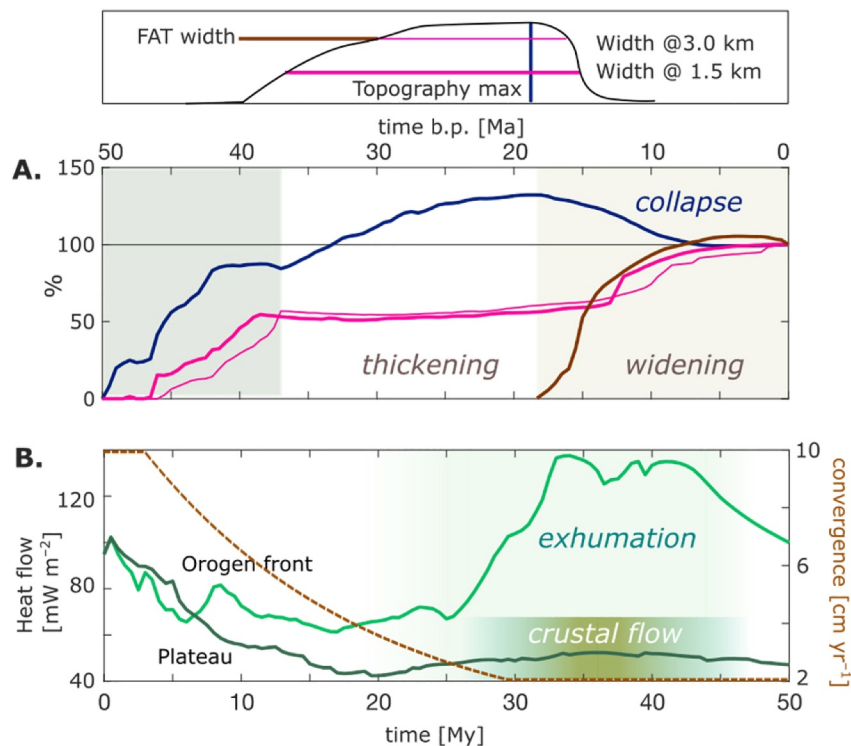


Figure 10. Evolution of (a) height (blue) of the orogeny, width measured at 3 and 1.5 km height of the wedge (magenta), and the fold-and-thrust belt (FAT, brown) with respect to the final stage. (b) Maximum heat flow in the orogen front (light green) and in the plateau domain (dark green), and convergence velocity (brown). Exhumation coincides with increased heat flow in the orogenic front.

Models proposed for the plateau collapse invoked the dissipation of excess potential energy, relating extension to variations of boundary conditions (C. Wang et al., 2014, and references therein). Here, the models have shown that indeed the slowing India-Asia convergence lowers the dynamic support of the elevated edifice, allowing release of potential energy, lowering altitudes as Tibet undergoes extension. We find that the critical velocity, for the given quartzite rheology, to reorganize the orogen is around 5 cm yr^{-1} , whilst the gravitational collapse and relaxation of the orogen occurs at a velocity of $\sim 3 \text{ cm}$.

5. Conclusions

A notable feature of the India-Asia relative motions is the prolonged decrease in convergence velocity during the Himalayan-Tibetan orogeny. This study uses a thermo-mechanical model to examine the impact of decreasing convergence on orogenic structuring and subducting lithosphere. We emphasize the role of convergence velocity using the same lithospheric mantle and crustal rheology across the colliding margin and testing models with constant convergence velocity. The models show that the evolution resulting from decreasing convergence velocity is remarkably different from an orogeny achieved at constant rates. At high constant convergence velocity, the subducting crust is buried and then emplaced along the Moho of the upper plate crust, causing uplift of the overriding crust with minimal internal deformation. The buried and injected crust is then exhumed to the front of the orogeny through return flow. At low constant convergence velocity, folding and faulting are the dominant structural styles, yet neither exhumation nor return flow occurs. Although the modeled decreasing convergence velocity encompasses these two rheological end members, creep-dominated versus plasticity-dominated, the models with slowing convergence below 5 cm yr^{-1} develop a remarkably different evolution. Structures formed early, similar to those of fast convergence, are then abandoned or overprinted, as convergence velocity decreases. This occurs during a transient phase that shifts the system toward a new equilibrium that occurs at a velocity below 5 cm yr^{-1} , as basal shearing and compression decrease, allowing thermal re-equilibration and flow. This triggers a second stage, in which the orogeny widens as a fold-and-thrust belt form at the front. A third stage is found as the convergence velocity further decrease below $\sim 3 \text{ cm yr}^{-1}$, when compressional forces decrease and

can no longer sustain the thick orogen, therefore allowing relaxation and “collapse” of the plateau, reflected by a decrease in topography and ascent of deeply buried crust. The models capture many features of the collisional zone, that is, the Himalayan crustal exhumation and return flow, the fold and thrust belt formation against the southern Tibet and the late stage of doming and current inner extension. These three stages are explained by decreasing convergence models reproducing the fast early growth of the Tibetan Plateau, its widening and late-stage collapse, behind an expanding Himalayan fold-and-thrust belt, providing insights into the evolution of such a complex collisional margin.

Conflict of Interest

The authors declare no conflicts of interest relevant to this study.

Data Availability Statement

The software used for this research (Underworld2) is available from Beucher et al. (2019), licensed under LGPL Version 3. A script to replicate the research presented is available at Knight (2024), licensed under Creative Commons Attribution 4.0 International, with model parameters for all models outlined in Table S2 in Supporting Information S1. Data from EarthEnv-DEM90 (Robinson et al., 2014), licensed under a Creative Commons Attribution 4.0 International License, and HimTibetMap (Styron et al., 2010), licensed under an open data commons attribution license, were used in the creation of figures. Figures were made with Matplotlib (Caswell et al., 2020), available under the Matplotlib license at <https://matplotlib.org/>. Maps were created using the software Cartopy (Elson et al., 2024), licensed under the 3-Clause BSD license.

Acknowledgments

The authors acknowledge and pay our respects to the Kulin Nation (Monash) and Whadjuk Nyungar people (Curtin) who are the Traditional Custodians of the land this research was conducted on. We acknowledge support from Australian Research Council Grants FT170100254 (awarded to F.A.C) and FT220100566 (supporting B.S.K). L.D.Z. was supported by the Earth Observatory of Singapore (EOS), and the Singapore Ministry of Education Tier 3b project “Investigating Volcano and Earthquake Science and Technology (InVEST)” (Award number MOE-MOET32021-0002). The authors acknowledge AuScope for their continued support in the development of the Underworld code. The authors acknowledge the provision of resources and services from the National Computational Infrastructure (NCI), which is supported by the Australian Government. The authors would like to thank reviewers Ana M. Negredo, Anne Replumaz and an anonymous reviewer for detailed comments that greatly improved the manuscript.

References

- Ader, T., Avouac, J.-P., Liu-Zeng, J., Lyon-Caen, H., Bollinger, L., Galetzka, J., et al. (2012). Convergence rate across the Nepal Himalaya and interseismic coupling on the Main Himalayan Thrust: Implications for seismic hazard: Coupling on the MHT. *Journal of Geophysical Research*, 117(B4). <https://doi.org/10.1029/2011JB009071>
- Beaumont, C., Jamieson, R. A., Nguyen, M. H., & Lee, B. (2001). Himalayan tectonics explained by extrusion of a low-viscosity crustal channel coupled to focused surface denudation. *Nature*, 414(6865), 738–742. <https://doi.org/10.1038/414738a>
- Beucher, R., Moresi, L., Giordani, J., Mansour, J., Sandiford, D., Farrington, R., et al. (2019). UWGeodynamics: A teaching and research tool for numerical geodynamic modelling [Software]. *Journal of Open Source Software*, 4(36), 1136. <https://doi.org/10.21105/joss.01136>
- Burchfiel, B. C., Zhiliang, C., Hodges, K. V., Yuping, L., Royden, L. H., Changrong, D., & Jiene, X. (1992). The South Tibetan detachment system, Himalayan Orogen: Extension contemporaneous with and parallel to shortening in a collisional mountain belt. In B. C. Burchfiel, C. Zhiliang, K. V. Hodges, L. Yuping, L. H. Royden, D. Changrong, et al. (Eds.), *The South Tibetan detachment system, Himalayan Orogen: Extension contemporaneous with and parallel to shortening in a collisional mountain belt*. Geological Society of America. <https://doi.org/10.1130/SPE269-p1>
- Caswell, T., Drostboom, M., Lee, A., Hunter, J., Firing, E., Stansby, D., et al. (2020). Matplotlib v3.2.1 [Software]. Zenodo. <https://doi.org/10.5281/zenodo.3714460>
- Chen, L., Capitanio, F. A., Liu, L., & Gerya, T. V. (2017). Crustal rheology controls on the Tibetan Plateau formation during India-Asia convergence. *Nature Communications*, 8(1), 15992. <https://doi.org/10.1038/ncomms15992>
- Clark, M. K., & Royden, L. H. (2000). Topographic ooze: Building the eastern margin of Tibet by lower crustal flow 4.
- DeCelles, P. G., Robinson, D. M., Quade, J., Ojha, T. P., Garzione, C. N., Copeland, P., & Upreti, B. N. (2001). Stratigraphy, structure, and tectonic evolution of the Himalayan fold-thrust belt in western Nepal. *Tectonics*, 20(4), 487–509. <https://doi.org/10.1029/2000TC001226>
- DeCelles, P. G., Robinson, D. M., & Zandt, G. (2002). Implications of shortening in the Himalayan fold-thrust belt for uplift of the Tibetan Plateau. *Tectonics*, 21(6), 12-1–12-25. <https://doi.org/10.1029/2001TC001322>
- de Sigoyer, J., Chavagnac, V., Blichert-Toft, J., Villa, I. M., Luais, B., Guillot, S., et al. (2000). Dating the Indian continental subduction and collisional thickening in the northwest Himalaya: Multichronology of the Tso Morari eclogites. *Geology*, 28(6), 487–490. [https://doi.org/10.1130/0091-7613\(2000\)28<487:DTICSA>2.0.CO;2](https://doi.org/10.1130/0091-7613(2000)28<487:DTICSA>2.0.CO;2)
- Ding, L., Kapp, P., Cai, F., Garzione, C. N., Xiong, Z., Wang, H., & Wang, C. (2022). Timing and mechanisms of Tibetan Plateau uplift. *Nature Reviews Earth & Environment*, 3(10), 652–667. <https://doi.org/10.1038/s43017-022-00318-4>
- Elson, P., de Andrade, E. S., Lucas, G., May, R., Hattersley, R., Campbell, E., et al. (2024). SciTools/cartopy: REL: v0.24.1 [Software]. <https://doi.org/10.5281/zenodo.13905945>
- England, P., & Molnar, P. (2005). Late Quaternary to decadal velocity fields in Asia. *Journal of Geophysical Research*, 110(B12). <https://doi.org/10.1029/2004JB003541>
- Faccenda, M., Gerya, T. V., & Chakraborty, S. (2008). Styles of post-subduction collisional orogeny: Influence of convergence velocity, crustal rheology and radiogenic heat production. *Lithos*, 103(1–2), 257–287. <https://doi.org/10.1016/j.lithos.2007.09.009>
- Faccenda, M., Minelli, G., & Gerya, T. V. (2009). Coupled and decoupled regimes of continental collision: Numerical modeling. *Earth and Planetary Science Letters*, 278(3–4), 337–349. <https://doi.org/10.1016/j.epsl.2008.12.021>
- Finch, M., Hasalová, P., Weinberg, R. F., & Fanning, C. M. (2014). Switch from thrusting to normal shearing in the Zanskar shear zone, NW Himalaya: Implications for channel flow. *Geological Society of America Bulletin*, 126(7–8), 892–924. <https://doi.org/10.1130/B30817.1>
- Gao, R., Lu, Z. W., Klemperer, S. L., Wang, H. Y., Dong, S. W., Li, W. H., & Li, H. Q. (2016). Crustal-scale duplexing beneath the Yarlung Zangbo suture in the western Himalaya. *Nature Geoscience*, 9(7), 555–560. <https://doi.org/10.1038/ngeo2730>

- Gerya, T. V., Perchuk, L. L., & Burg, J.-P. (2008). Transient hot channels: Perpetrating and regurgitating ultrahigh-pressure, high-temperature crust–mantle associations in collision belts. *Lithos*, 103(1–2), 236–256. <https://doi.org/10.1016/j.lithos.2007.09.017>
- Gibbons, A. D., Zahirovic, S., Müller, R. D., Whittaker, J. M., & Yatheesh, V. (2015). A tectonic model reconciling evidence for the collisions between India, Eurasia and intra-oceanic arcs of the central-eastern Tethys. *Gondwana Research*, 28(2), 451–492. <https://doi.org/10.1016/j.gr.2015.01.001>
- Godin, L., Grujic, D., Law, R. D., & Searle, M. P. (2006). Channel flow, ductile extrusion and exhumation in continental collision zones: An introduction. *Geological Society, London, Special Publications*, 268, 1–23. <https://doi.org/10.1144/GSL.SP.2006.268.01.01>
- Goscombe, B., Gray, D., & Foster, D. A. (2018). Metamorphic response to collision in the Central Himalayan Orogen. *Gondwana Research*, 57, 191–265. <https://doi.org/10.1016/j.gr.2018.02.002>
- Grujic, D., Casey, M., Davidson, C., Hollister, L. S., Kündig, R., Pavlis, T., & Schmid, S. (1996). Ductile extrusion of the Higher Himalayan Crystalline in Bhutan: Evidence from quartz microfabrics. *Tectonophysics*, 260(1–3), 21–43. [https://doi.org/10.1016/0040-1951\(96\)00074-1](https://doi.org/10.1016/0040-1951(96)00074-1)
- Grujic, D., Warren, C. J., & Wooden, J. L. (2011). Rapid synconvergent exhumation of Miocene-aged lower orogenic crust in the eastern Himalaya. *Lithosphere*, 3(5), 346–366. <https://doi.org/10.1130/L154.1>
- Guillot, S., Garzanti, E., Baratoux, D., Marquer, D., Mahéo, G., & de Sigoyer, J. (2003). Reconstructing the total shortening history of the NW Himalaya. *Geochemistry, Geophysics, Geosystems*, 4(7). <https://doi.org/10.1029/2002GC000484>
- Hunter, N. J. R., Weinberg, R. F., Wilson, C. J. L., Luzin, V., & Misra, S. (2018). Microscopic anatomy of a “hot-on-cold” shear zone: Insights from quartzites of the Main Central Thrust in the Alaknanda region (Garhwal Himalaya). *Geological Society of America Bulletin*, 130(9–10), 1519–1539. <https://doi.org/10.1130/B31797.1>
- Ingalls, M., Rowley, D. B., Currie, B., & Colman, A. S. (2016). Large-scale subduction of continental crust implied by India–Asia mass-balance calculation. *Nature Geoscience*, 9(11), 848–853. <https://doi.org/10.1038/ngeo2806>
- Jagoutz, O., Müntener, O., Schmidt, M. W., & Burg, J.-P. (2011). The roles of flux- and decompression melting and their respective fractionation lines for continental crust formation: Evidence from the Kohistan arc. *Earth and Planetary Science Letters*, 303(1–2), 25–36. <https://doi.org/10.1016/j.epsl.2010.12.017>
- Jamieson, R. A., & Beaumont, C. (2013). On the origin of orogens. *Geological Society of America Bulletin*, 125(11–12), 1671–1702. <https://doi.org/10.1130/B30855.1>
- Jessup, M. J., Langille, J. M., Diedesch, T. F., & Cottle, J. M. (2019). Gneiss dome formation in the Himalaya and southern Tibet. *Geological Society, London, Special Publications*, 483(1), 401–422. <https://doi.org/10.1144/SP483.15>
- Jessup, M. J., Law, R. D., Searle, M. P., & Hubbard, M. S. (2006). Structural evolution and vorticity of flow during extrusion and exhumation of the Greater Himalayan Slab, Mount Everest Massif, Tibet/Nepal: Implications for orogen-scale flow partitioning. In R. D. Law, M. P. Searle, & L. Godin (Eds.), *Channel flow, ductile extrusion and exhumation in continental collision zones*. Geological Society of London. <https://doi.org/10.1144/GSL.SP.2006.268.01.18>
- Jiménez-Munt, I., Fernández, M., Vergés, J., & Platt, J. P. (2008). Lithosphere structure underneath the Tibetan Plateau inferred from elevation, gravity and geoid anomalies. *Earth and Planetary Science Letters*, 267(1–2), 276–289. <https://doi.org/10.1016/j.epsl.2007.11.045>
- Kelly, S., Beaumont, C., & Butler, J. P. (2019). Inherited terrane properties explain enigmatic post-collisional Himalayan-Tibetan evolution. *Geology*, 48(1), 8–14. <https://doi.org/10.1130/G46701.1>
- Klemperer, S. L. (2006). Crustal flow in Tibet: Geophysical evidence for the physical state of Tibetan lithosphere, and inferred patterns of active flow. *Geological Society, London, Special Publications*, 268(1), 39–70. <https://doi.org/10.1144/GSL.SP.2006.268.01.03>
- Knight, B. S. (2024). Underworld-community/Knight-Himalayas: India-Asia collision reconstruction (v1.1.1) [ComputationalNotebook]. Zenodo. <https://doi.org/10.5281/zenodo.14263140>
- Knight, B. S., Capitanio, F. A., & Weinberg, R. F. (2021). Convergence velocity controls on the structural evolution of orogens. *Tectonics*, 40(9), e2020TC006570. <https://doi.org/10.1029/2020TC006570>
- Kumar, P., Tewari, H. C., & Sreenivas, B. (2019). Seismic structure of the central Indian crust and its implications on the crustal evolution. *Journal of the Geological Society of India*, 93(2), 163–170. <https://doi.org/10.1007/s12594-019-1146-4>
- Lee, J., Hacker, B. R., Dinklage, W. S., Wang, Y., Gans, P., Calvert, A., et al. (2000). Evolution of the Kangmar Dome, southern Tibet: Structural, petrologic, and thermochromologic constraints. *Tectonics*, 19(5), 872–895. <https://doi.org/10.1029/1999TC001147>
- Lee, T.-Y., & Lawyer, L. A. (1995). Cenozoic plate reconstruction of Southeast Asia. *Tectonophysics, Southeast Asia Structure and Tectonics*, 251(1–4), 85–138. [https://doi.org/10.1016/0040-1951\(95\)00023-2](https://doi.org/10.1016/0040-1951(95)00023-2)
- Li, Z.-H., Liu, M., & Gerya, T. (2016). Lithosphere delamination in continental collisional orogens: A systematic numerical study. *Journal of Geophysical Research: Solid Earth*, 121(7), 5186–5211. <https://doi.org/10.1002/2016JB013106>
- Liang, S., Gan, W., Shen, C., Xiao, G., Liu, J., Chen, W., et al. (2013). Three-dimensional velocity field of present-day crustal motion of the Tibetan Plateau derived from GPS measurements. *Journal of Geophysical Research: Solid Earth*, 118(10), 5722–5732. <https://doi.org/10.1002/2013JB010503>
- Liu, L., Liu, L., Morgan, J. P., Xu, Y.-G., & Chen, L. (2023). New constraints on Cenozoic subduction between India and Tibet. *Nature Communications*, 14(1), 1963. <https://doi.org/10.1038/s41467-023-37615-5>
- Lu, H., Tian, X., Yun, K., & Li, H. (2018). Convective removal of the Tibetan Plateau mantle lithosphere by ~26 Ma. *Tectonophysics*, 731–732, 17–34. <https://doi.org/10.1016/j.tecto.2018.03.006>
- Maiti, G., & Mandal, N. (2021). Early Miocene exhumation of high-pressure rocks in the Himalaya: A response to reduced India-Asia convergence velocity. *Frontiers of Earth Science*, 9. <https://doi.org/10.3389/feart.2021.632806>
- Mansour, J., Giordani, J., Moretti, L., Beucher, R., Kaluza, O., Velic, M., et al. (2020). Underworld2: Python geodynamics modelling for Desktop, HPC and Cloud. *Journal of Open Source Software*, 5(47), 1797. <https://doi.org/10.21105/joss.01797>
- Meng, J., Gilder, S. A., Wang, C., Coe, R. S., Tan, X., Zhao, X., & He, K. (2019). Defining the limits of greater India. *Geophysical Research Letters*, 46(8), 4182–4191. <https://doi.org/10.1029/2019GL082119>
- Mitsuishi, M., Wallis, S. R., Aooya, M., Lee, J., & Wang, Y. (2012). E–W extension at 19 Ma in the Kung Co area, S. Tibet: Evidence for contemporaneous E–W and N–S extension in the Himalayan orogen. *Earth and Planetary Science Letters*, 325–326, 10–20. <https://doi.org/10.1016/j.epsl.2011.11.013>
- Molnar, P., & Stock, J. M. (2009). Slowing of India's convergence with Eurasia since 20 Ma and its implications for Tibetan mantle dynamics. *Tectonics*, 28(3). <https://doi.org/10.1029/2008TC002271>
- Molnar, P., & Tapponnier, P. (1975). Cenozoic tectonics of Asia: Effects of a continental collision. *Science*, 189(4201), 419–426. <https://doi.org/10.1126/science.189.4201.419>
- Müller, R. D., Sdrolias, M., Gaina, C., & Roest, W. R. (2008). Age, spreading rates, and spreading asymmetry of the world's ocean crust. *Geochemistry, Geophysics, Geosystems*, 9(4). <https://doi.org/10.1029/2007GC001743>

- Nelson, K. D., Zhao, W., Brown, L. D., Kuo, J., Che, J., Liu, X., et al. (1996). Partially molten middle Crust Beneath Southern Tibet: Synthesis of project INDEPTH results. *Science*, 274(5293), 1684–1688. <https://doi.org/10.1126/science.274.5293.1684>
- Piccolo, A., Faccenda, M., Carosi, R., Montomoli, C., & Visonà, D. (2017). Crustal strength control on structures and metamorphism in collisional orogens. *Tectonophysics*, 746, 470–492. <https://doi.org/10.1016/j.tecto.2017.09.018>
- Pichon, X. L., Fournier, M., & Jolivet, L. (1992). Kinematics, topography, shortening, and extrusion in the India-Eurasia collision. *Tectonics*, 11(6), 1085–1098. <https://doi.org/10.1029/92TC01566>
- Replumaz, A., Kárasón, H., Van Der Hilst, R. D., Besse, J., & Tapponnier, P. (2004). 4-D evolution of SE Asia's mantle from geological reconstructions and seismic tomography. *Earth and Planetary Science Letters*, 221(1–4), 103–115. [https://doi.org/10.1016/S0012-821X\(04\)00070-6](https://doi.org/10.1016/S0012-821X(04)00070-6)
- Replumaz, A., Negredo, A. M., Guillot, S., van der Beek, P., & Villaseñor, A. (2010). Crustal mass budget and recycling during the India/Asia collision. *Tectonophysics*, 492(1–4), 99–107. <https://doi.org/10.1016/j.tecto.2010.05.023>
- Robinson, N., Regetz, J., & Guralnick, R. P. (2014). EarthEnv-DEM90: A nearly-global, void-free, multi-scale smoothed, 90 m digital elevation model from fused ASTER and SRTM data [Dataset]. *ISPRS Journal of Photogrammetry and Remote Sensing*, 87, 57–67. <https://doi.org/10.1016/j.isprsjprs.2013.11.002>
- Rowley, D. B. (1996). Age of initiation of collision between India and Asia: A review of stratigraphic data. *Earth and Planetary Science Letters*, 145(1–4), 1–13. [https://doi.org/10.1016/S0012-821X\(96\)00201-4](https://doi.org/10.1016/S0012-821X(96)00201-4)
- Royden, L. H., Burchfiel, B. C., King, R. W., Wang, E., Chen, Z., Shen, F., & Liu, Y. (1997). Surface deformation and lower crustal flow in eastern Tibet. *Science*, 276(5313), 788–790. <https://doi.org/10.1126/science.276.5313.788>
- Searle, M. P. (2015). Mountain building, tectonic evolution, rheology, and crustal flow in the Himalaya, Karakoram, and Tibet. In *Treatise on Geophysics* (pp. 469–511). Elsevier. Elsevier. <https://doi.org/10.1016/B978-0-444-53802-4.00121-4>
- Searle, M. P., & Hacker, B. R. (2019). Structural and metamorphic evolution of the Karakoram and Pamir following India–Kohistan–Asia collision. *Geological Society, London, Special Publications*, 483(1), 555–582. <https://doi.org/10.1144/SP483.6>
- Sizova, E., Gerya, T., & Brown, M. (2012). Exhumation mechanisms of melt-bearing ultrahigh pressure crustal rocks during collision of spontaneously moving plates. *Journal of Metamorphic Geology*, 30(9), 927–955. <https://doi.org/10.1111/j.1525-1314.2012.01004.x>
- Spain, M., & Hirn, A. (1997). Seismic structure and evidence for eclogitization during the Himalayan convergence. *Tectonophys*, 273(1–2), 1–16.
- Collisional Orogenes Zones Act. Transf. Crust Mantle, Collisional Orogenes: Zones of Active Transfer Between Crust and Mantle. [https://doi.org/10.1016/S0040-1951\(96\)00285-5](https://doi.org/10.1016/S0040-1951(96)00285-5)
- Streule, M. J., Strachan, R. A., Searle, M. P., & Law, R. D. (2010). Comparing Tibet-Himalayan and Caledonian crustal architecture, evolution and mountain building processes. *Geological Society, London, Special Publications*, 335(1), 207–232. <https://doi.org/10.1144/SP335.10>
- Styron, R., Taylor, M., & Okoronkwo, K. (2010). HimaTibetMap-1.0: New “web-2.0” online database of active structures from the Indo-Asian collision [Dataset]. *Eos*, 91(20), 181–182. <https://doi.org/10.1029/2010eo200001>
- Tapponnier, P., Zhiqin, X., Roger, F., Meyer, B., Arnaud, N., Wittlinger, G., & Jingsui, Y. (2001). Oblique stepwise rise and growth of the Tibet Plateau. *Science*, 294(5547), 1671–1677. <https://doi.org/10.1126/science.105978>
- Taylor, M., & Yin, A. (2009). Active structures of the Himalayan-Tibetan orogen and their relationships to earthquake distribution, contemporary strain field, and Cenozoic volcanism [Dataset]. *Geosphere*, 5(3), 199–214. <https://doi.org/10.1130/ges00217.s1>
- Unsworth, M. J., Jones, A. G., Wei, W., Marquis, G., Gokarn, S. G., Spratt, J. E., et al. (2005). Crustal rheology of the Himalaya and Southern Tibet inferred from magnetotelluric data. *Nature*, 438(7064), 78–81. <https://doi.org/10.1038/nature04154>
- van Hinsbergen, D. J. J., Kapp, P., Dupont-Nivet, G., Lippert, P. C., DeCelles, P. G., & Torsvik, T. H. (2011). Restoration of Cenozoic deformation in Asia and the size of Greater India. *Tectonics*, 30(5). <https://doi.org/10.1029/2011TC002908>
- Vogt, K., Matenco, L., & Cloetingh, S. (2017). Crustal mechanics control the geometry of mountain belts. Insights from numerical modelling. *Earth and Planetary Science Letters*, 460, 12–21. <https://doi.org/10.1016/j.epsl.2016.11.016>
- Wang, C., Dai, J., Zhao, X., Li, Y., Graham, S. A., He, D., et al. (2014). Outward-growth of the Tibetan Plateau during the Cenozoic: A review. *Tectonophysics*, 621, 1–43. <https://doi.org/10.1016/j.tecto.2014.01.036>
- Wang, L., & Barbot, S. (2023). Three-dimensional kinematics of the India–Eurasia collision. *Communications Earth & Environment*, 4(1), 164. <https://doi.org/10.1038/s43247-023-00815-4>
- Warren, C. J., Beaumont, C., & Jamieson, R. A. (2008). Deep subduction and rapid exhumation: Role of crustal strength and strain weakening in continental subduction and ultrahigh-pressure rock exhumation. *Tectonics*, 27(6). <https://doi.org/10.1029/2008TC002292>
- Willett, S. D., & Beaumont, C. (1994). Subduction of Asian lithospheric mantle beneath Tibet inferred from models of continental collision. *Nature*, 369(6482), 642–645. <https://doi.org/10.1038/369642a0>
- Yakovlev, P. V., & Clark, M. K. (2014). Conservation and redistribution of crust during the Indo-Asian collision. *Tectonics*, 33(6), 1016–1027. <https://doi.org/10.1002/2013TC003469>
- Yin, A., & Harrison, T. M. (2000). Geologic evolution of the Himalayan-Tibetan orogen. *Annual Review of Earth and Planetary Sciences*, 28(1), 211–280. <https://doi.org/10.1146/annurev.earth.28.1.211>
- Zhao, Q., Chen, Q., van Dam, T., She, Y., & Wu, W. (2023). The vertical velocity field of the Tibetan Plateau and its surrounding areas derived from GPS and surface mass loading models. *Earth and Planetary Science Letters*, 609, 118107. <https://doi.org/10.1016/j.epsl.2023.118107>
- Zhao, W., Nelson, K. D., Che, J., Quo, J., Lu, D., Wu, C., & Liu, X. (1993). Deep seismic reflection evidence for continental underthrusting beneath southern Tibet. *Nature*, 366(6455), 557–559. <https://doi.org/10.1038/366557a0>
- Zhao, W.-L., & Morgan, W. J. (1987). Injection of Indian crust into Tibetan lower crust: A two-dimensional finite element model study. *Tectonics*, 6(4), 489–504. <https://doi.org/10.1029/TC006i004p00489>